JPhys Materials

PAPER • OPEN ACCESS

Photonics design theory enhancing light extraction efficiency in quantum dot light emitting diodes

To cite this article: Diyar Mousa Othman *et al* 2022 *J. Phys. Mater.* **5** 044009

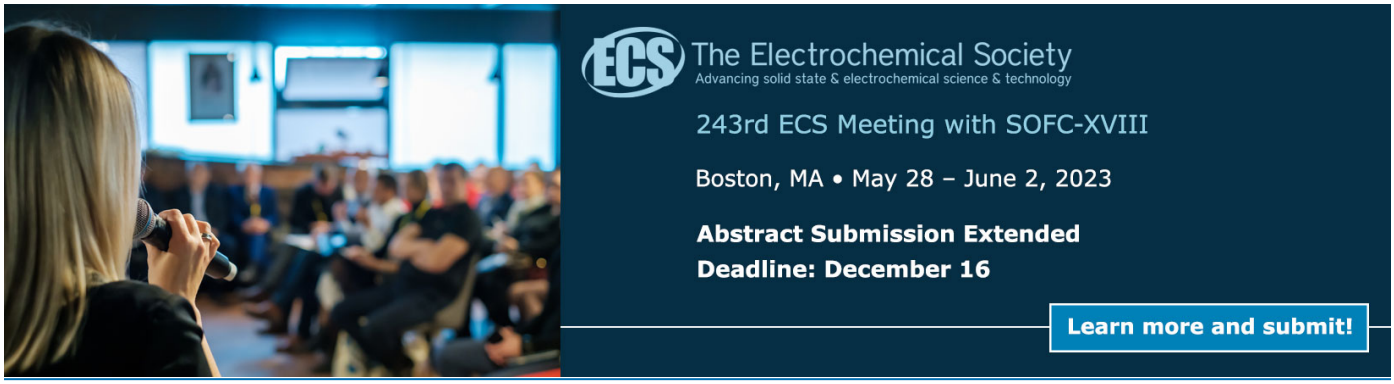

Journal of Physics: Materials

PAPER

Photonics design theory enhancing light extraction efficiency in quantum dot light emitting diodes

Diyar Mousa Othman[1], Julia A Weinstein[2], Quan Lyu[3,*] and Bo Hou[1,*]

[1] School of Physics and Astronomy, Cardiff University, Cardiff CF24 3AA, United Kingdom
[2] Department of Chemistry, The University of Sheffield, Sheffield, S3 7HF, United Kingdom
[3] Cambridge Research Centre, Huawei Technologies Research & Development (UK) Ltd, Cambridge, CB4 0FY, United Kingdom
* Authors to whom any correspondence should be addressed.

E-mail: lyuquan@huawei.com and Houb6@cardiff.ac.uk

Keywords: photonics, design, extraction, efficiency, LED, quantum dot

OPEN ACCESS

RECEIVED
19 September 2022

REVISED
24 October 2022

ACCEPTED FOR PUBLICATION
28 October 2022

PUBLISHED
8 November 2022

Abstract

The external quantum efficiency (EQE) of quantum dot light emitting diodes (QLEDs) needs improvement for more power-efficient devices. One of the main limitations is the low light extraction efficiency (LEE). Generally, only 20% of the light that is generated inside the emissive layer makes its way out of the device into air, with the rest being lost to waveguide and substrate modes and surface plasmon polaritons. Different photonics structures have been previously tested to help extract the light that is trapped inside the device. Here we report a photonics design which is a combination of nanopillars and grating structures for improving the LEE of QLEDs. The effect of changing the nanopillar height, radius and material has been studied. It was found that ZnO nanopillars of 500 nm pitch, 200 nm height and 400 nm width alongside 150 nm width and pitch grating structure can increase the LEE at 460 nm by 50% and at 640 nm by 20%. It was also found that different materials can help extract light at different wavelengths. TiO_2 nanopillars increased the extraction efficiency at ∼590 nm region which was not observed by the other materials. As around 19% of the world's electricity consumption is due to lighting applications, increasing the LEE can significantly reduce the power consumption.

1. Introduction

Solution-processed light emitting diodes (LEDs) have been the state-of-the-art emerging technology for displays and ambient lighting [1, 2]. They are desirable due to their low-cost fabrication processes, wide viewing angles and electroluminescent operation modes, which eliminate the need for a backlight and result in very thin devices [3]. However, the organic materials used to fabricate the devices have short lifetimes when compared to inorganic materials, so organic LEDs (OLEDs), especially blue ones, suffer from a short lifespan due to their sensitivity against oxygen and moisture [4, 5]. In addition, they have problems like burn-ins which occur when the same contents are displayed for extended periods of time [6]. Quantum dots (QDs) are a possible replacement for light emitters due to their tunable bandgap [7], colour purity [8], higher stability [9], low cost and solution processability [10]. Even though they made their way into the market under the name of quantum dot LEDs (QLEDs), commercialized QLED displays still use backlight to excite QDs which is the photoluminescent mode lighting, similar to that of an LCD [11]. Recently, significant research has been made to increase the efficiency of electroluminescent QLEDs (EL-QLEDs) to be able to fabricate active pixelated QLEDs for display and lighting applications [1, 2].

Improving the quantum efficiency of lighting devices is considerably important in a world where energy supply and consumption is becoming a problem [12]. Roughly 19% of the total electricity consumption in the world is used for lighting applications, of which 40%–45% is LED, OLED and similar technologies [13]. This number is increasing everyday and for this reason, the demand for more power-efficient devices is increasing for a more sustainable and low carbon footprint future. The external quantum efficiency (EQE), which is the ratio of the number of photons that make their way out into air to the number of electron–hole

pairs injected into the device, has surpassed 20% for EL-QLEDs [14, 15]. The EQE of a device is given by the formula [16]

$$\mathrm{EQE} = \mathrm{LEE} \times \mathrm{IQE} = \mathrm{LEE} \times q_{\mathrm{eff}} \times \eta_{S/T} \times \gamma \tag{1}$$

where IQE is the internal quantum efficiency and is a product of the effective quantum efficiency q_{eff}, the singlet to triplet capture ratio $\eta_{S/T}$ and a constant γ which is dependent on the charge carrier balance and exciton quenching. It is sometimes stated that the IQE reaches 100% for some devices, but this is generally a measure of photoluminescence quantum yield (PLQY)—a material characteristic, instead of IQE, which is a device characteristic [17]. One of the biggest challenges with EL-QLED devices is the light extraction efficiency (LEE) [18]. The LEE of a typical stack is around 20% [19], and so LEE is sometimes assumed to be 20% and used along with the EQE to approximate the IQE [20, 21]. It is important to understand and differentiate the LEE factors affecting the EQE to be able to improve them. In addition, the use of two different LEE enhancing structures in two different interfaces has also not been reported so far. Herein, this work focuses on improving the LEE of these devices, whereas the focus on other aspects will be done in the works to follow. We found that using a grating structure in the transparent conducting electrode and glass interface in addition to a photonics nanopillar structure on top of the glass layer can increase the LEE in short wavelengths by up to 50%. The effect of using different dielectric materials for nanopillars was also studied. It was found that it is possible to increase the LEE in different regions by altering the nanopillar dimensions and materials.

2. Theoretical background

To understand why only a fraction of light makes its way into air, it is important to understand the structure of these QLED devices. A typical QLED device consists of five main layers. These are the anode, the hole transport layer (HTL), the emissive layer (EML), the electron transport layer (ETL) and the cathode. The anode and the cathode act as the source of holes and electrons respectively. The HTL and ETL transport the holes and electrons to the EML, where they recombine to produce photons with energy equal to the bandgap of the EML material. Additional layers like the hole injection layer (HIL) and the electron injection layer can be used in between the source and the transport layers to increase the injection efficiency of charge carriers into the EML [22]. In addition, a glass layer is also found on top of the electrode at which light leaves the structure and is often used as a substrate. All of these layers are stacked up on top of each other in order, and the photons are produced in the middle of the stack. Therefore, there are multiple boundaries the photons have to go through for the light to make its way into the air. The EL-QLED structure is very similar to that of an OLED, with the difference coming from the EML being made out of QDs and the ETL being made out of inorganic materials, mostly metal oxides such as ZnO, SnO_2 and TiO_2 [23–25]. The typical parameters of different QLED layers used in this work can be seen in table 1.

One of the ways light is lost inside the stack is through waveguide and substrate modes. The reflective metal electrode and the glass substrate have lower refractive indices compared to the functional materials that make up the HTL, ETL and EML. In simple terms, this results in the glass and the metal electrode acting like the cladding, and the middle layers acting like the core of an optical fibre which supports waveguide modes. When the stack thickness is put into account, it is found that both transverse electric (TE) and transverse magnetic (TM) modes are supported inside the stack [44]. This is further explained in the following chapter. Most of these modes propagate tangentially to the layers, meaning the light does not make its way out of the structure and is lost. Another way light is lost is via total internal reflection (TIR) which is the main reason the waveguide modes are formed in the first place. TIR takes place at interfaces where light travels from a medium with a higher refractive index to a medium with a lower refractive index. If the angle that the light is travelling with respect to the normal to the interface is greater than some certain angle, TIR takes place and the light is reflected back into the medium. This angle is called the critical angle and is given by the equation

$$\sin(\theta_C) = \frac{n_2}{n_1} \tag{2}$$

where n_2 is the refractive index of the less dense medium and n_1 is the refractive index of the more dense medium. TIR can be observed in all the interfaces travelling outwards from the EML which adds to the waveguide mode losses. A process that also contributes to the loss is surface plasmon polaritons (SPPs). SPPs are charge density oscillations that take place at a metal-dielectric interface as a result of electromagnetic excitations of electrons in the conduction band of the metal [45]. The electric field that forms, as a result, can

Table 1. The typical parameters of the layers of a QLED stack.

Layer	Material	Thickness	Refractive Index (400–700 nm)
Cathode	Aluminium	15–100 nm [26, 27]	0.56–1.63 [28]
	Silver		—
ETL	ZnO nanoparticles	60–100 nm [29, 30]	1.69–1.62 [31]
	Doped ZnO nanoparticles		—
QD EML	Perovskite	20 nm [32–34]	—
	CdSe (Cd-Based)		2.55–2.57 [35]
	Cd-Free		—
HTL	TFB	20–40 nm [36–38]	—
	PVK		—
	CBP		1.70
HIL	MoO_3	5 nm	2.40–2.06 [39]
Anode	ITO	40–140 nm [40–42]	2.04–1.71 [43]

travel hundreds of nanometers into its surrounding media, decaying exponentially [46]. SPPs have high wavenumbers given by the equation [45]

$$k_{\text{spp}} = k_0\sqrt{\frac{\varepsilon_m\varepsilon_d}{\varepsilon_m+\varepsilon_d}} \tag{3}$$

where $k_0 = \omega/c$ is the free space wavenumber and ε_m and ε_d are the complex dielectric permittivity of the metal and the dielectric layer respectively. Since the wavenumbers of the SPPs are larger than the free space wavenumber, they can not be outcoupled into the air directly and therefore are dissipated [47].

There are multiple ways to improve the power output and efficiency of QLED devices. The most efficient change that can be made to these structures is decreasing the refractive indices of the layers sandwiched between the electrodes. Previous simulations show that using an EML with a refractive index of 1 would increase the theoretical limit of light extracted into air to 70% [48]. Even though it is challenging, research into new ETL, EML and HTL materials with lower refractive indices can still increase the EQE significantly.

A lot of research has been done on photonic structures that help increase the light extracted from the devices. Different microstructures like microlens arrays [49], scattering layers [50] and diffraction gratings [51] have previously been tested and proven to help the LEE of these devices. For example, the diffraction gratings help decrease the wavenumber of the waveguide or SPP modes according to the equation

$$k_0\sin\theta = k_{wg} \pm mk_G \tag{4}$$

where k_0 and θ are the wavenumber and exit angle of the light in free space, k_{wg} is the waveguide vector and $k_G = 2\pi/d$ is the grating vector of period d [52]. This decrease in the wavenumber allows the light to escape into air.

3. Simulation background

Finite-difference time domain (FDTD) was used to simulate the behaviour of electromagnetic fields inside of a QLED structure. FDTD is a method that uses Maxwell's equations to solve electrodynamics problems. It uses Yee's method proposed in 1966 [53]. It is a grid-based method that works by discretizing Maxwell's equations into their partial derivatives in space and time. The set of finite-difference equations can then be used to calculate one of the electromagnetic fields at a given instant of time. The solution to that can be used to solve for the remaining field in the next instant of time. This process is repeated until the steady-state electromagnetic fields are calculated, which are solutions to Maxwell's equations.

Maxwell's curl equations in a non-magnetic medium are given by

$$\nabla\times\vec{E} = \frac{\partial\vec{B}}{\partial t} \tag{5}$$

$$\nabla\times\vec{H} = -\frac{\partial\vec{D}}{\partial t} \tag{6}$$

where the magnetic flux density $\vec{B}$ is related to the magnetic field strength $\vec{H}$ with the equation $\vec{B} = \mu_0\mu_r(\omega)\vec{H}$ and the electric displacement field $\vec{D}$ is related to the electric field $\vec{E}$ with the equation $\vec{D} = \epsilon_0\epsilon_r(\omega)\vec{E}$. Electromagnetic field have six components in three dimensions which are the electric field

and magnetic field strength in x, y and z directions. For simplification, we make the assumption that the structure is infinite in one direction, e.g. z direction, and the fields are independent of z. The equations for the electromagnetic fields in the z direction and the relative permeability and permittivity can then be written as

$$\frac{\partial \overrightarrow{E}}{\partial z} = \frac{\partial \overrightarrow{H}}{\partial z} = 0. \tag{7}$$

$$\epsilon_r(\omega, x, y, z) = \epsilon_r(\omega, x, y) \tag{8}$$

$$\mu_r(\omega, x, y, z) = \mu_r(\omega, x, y). \tag{9}$$

This simplification splits Maxwell's equations into two sets of equations with three out of the 6 vector quantities in each, which can be solved in the x-y plane. These sets of equations are the TE and the TM modes of the electromagnetic radiation. The TM mode equations are reduced to

$$\frac{\partial D_z}{\partial t} = \frac{\partial H_y}{\partial x} - \frac{\partial H_x}{\partial y} \tag{10}$$

$$\frac{\partial H_x}{\partial t} = -\frac{1}{\mu_0}\frac{\partial E_z}{\partial y} \tag{11}$$

$$\frac{\partial H_y}{\partial t} = \frac{1}{\mu_0}\frac{\partial E_z}{\partial x}. \tag{12}$$

and these are similarly constructed for the TE modes. The partial differentials in equations (10)–(12) can all be approximated by using finite differences. By using the Taylor expansion of a function, the first derivative can be approximated by assuming a small deviation h. By neglecting higher order terms due to a small deviation, the first order differential can be expressed as

$$f'(x_0) \approx \frac{f(x_0 + h) - f(x_0 - h)}{2h}. \tag{13}$$

Each component is calculated at a slightly different point, all within a Yee cell. Yee cell is a staggered grid on which the components of the electromagnetic fields are calculated in 3D space. These fields are then interpolated by default to the origin of the cell. Repeating this process gives the steady state conditions of a system, which are approximated solutions to Maxwell's equations.

4. Experimental method

Nanopillar structured QLED [38] was used for the initial LEE simulations. The reference device consists of an Aluminium anode, MoO_3 HIL, 4,4′-Bis(N-carbazolyl)-1,1′-biphenyl (CBP) HTL, CdSe QDs EML, ZnO nanoparticles ETL, ITO cathode and glass. The structure is shown in figure 1. The thicknesses of these layers were cited from our previous works as 190 nm for the anode, 5 nm for the HIL, 60 nm for the HTL, 20 nm for the EML, 30 nm for the ETL, 100 nm for the cathode and 190 nm of glass [54–56]. The refractive indices for these layers were taken from table 1. The QD EML and the ZnO nanoparticle ETL were simulated as a thin film for simplicity. The device was stacked in the z axis. The approximation of the layer thicknesses, the values of the refractive indices and the assumption of the EML and ETL as a thin film may result in inaccuracies but have been carefully optimised and compared to real device.

We further investigated a new type of QLED photonic structure which combines grating and nanopillar arrays. The gratings are placed at the ITO/glass interface and the nanopillars are placed on top of a seed layer, which is above the glass layer as seen in figures 1(b) and 2. Two different structures are used at two different interfaces to try and extract more light from these interfaces and decrease the amount of TIR/waveguide modes that form inside the stack. The default material for the nanopillars and the seed layer below it is chosen to be ZnO as this was the material used by Yang *et al* [38]. The gratings have a width of 150 nm and a period of 300 nm. The nanopillars have a period of 500 nm, a radius of 100 nm and a height of 200 nm. The grating properties are kept the same throughout the simulation and the effect of changing the nanopillar radius, height and material are studied.

The simulation was run using a 3D FDTD solver (Lumerical package). The solver size in the x–y plane was 8 μm × 8 μm. The solver boundaries in the z-direction were from the middle of the metallic anode to about one micrometer above the glass layer. Perfectly matched layers (PML) boundaries were used for all of the boundaries except for the lower z boundary inside the metallic anode. PML boundaries absorb almost all

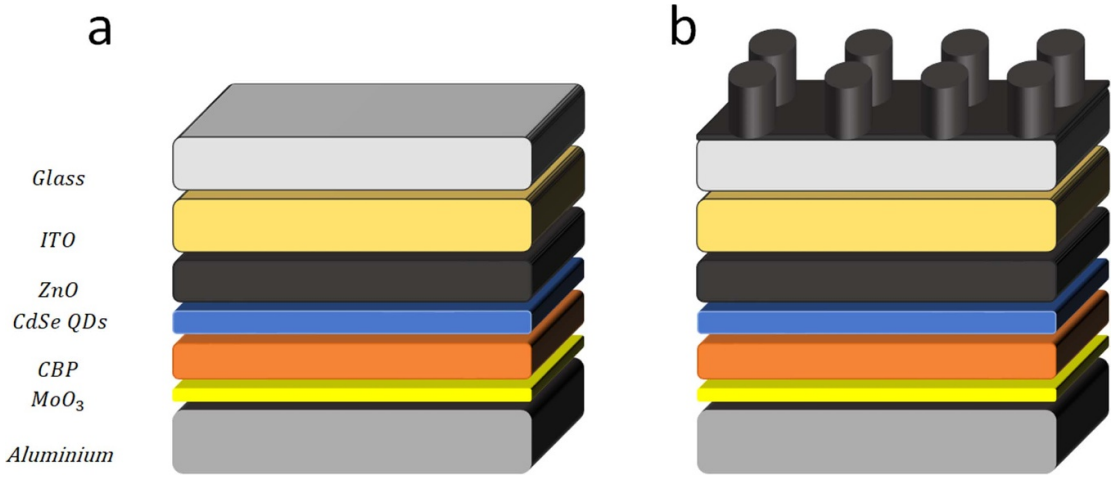

Figure 1. (a) The structure of the reference device showing the individual layers of the device stack, not to scale and (b) the addition of nanopillars on top of the glass layer.

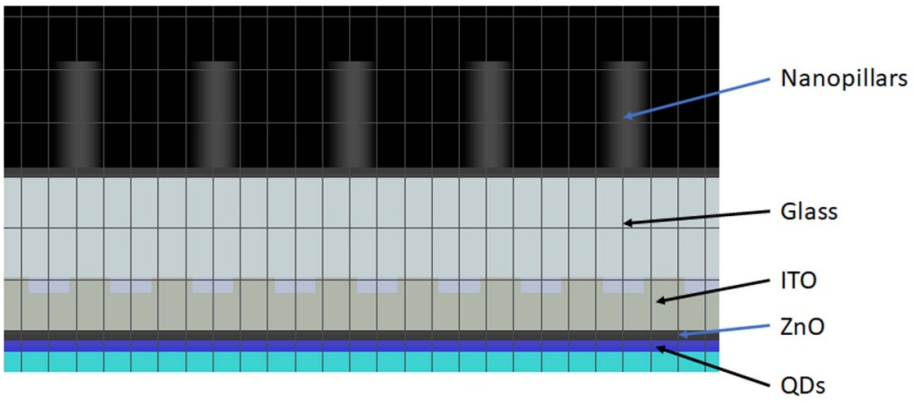

Figure 2. The grating structure at the ITO/glass interface and the nanopillars.

incoming radiation with minimal reflections, and since the light continues outwards from these boundaries in real life, it was important that no radiation was reflected back inside the simulation region. The lower z boundary was chosen to be metallic to reflect all the electromagnetic radiation coming towards it back inside the simulation region. Dipole sources were used to simulate the QDs in the EML. The electromagnetic fields produced by dipole sources are concentrated in the plane they are placed in, e.g. if the dipole is oriented in the z-axis, the emission will mainly be in the x–y plane. However, the photons produced by the recombination of electrons and holes inside QDs have a random direction, phase and polarization. To overcome this problem, the dipoles should be oriented on three different axes and the average electromagnetic field intensity can be calculated for isotropic, incoherent sources as

$$< |E|^2 >= \frac{|p_0|^2}{3}[|E_x|^2 + |E_y|^2 + |E_z|^2] \tag{14}$$

where E_x, E_y, and E_z represent the electromagnetic fields produced by the QD in three orientations. As FDTD is a coherent method, each dipole has to be simulated three times in different orientations and summed up incoherently, which is similar to using point-source radiators to simulate fluorescent molecules. In addition, dipoles should be placed along the active region as emissions can happen anywhere inside the EML. Even though it is impossible to simulate all positions in the EML, with enough dipole samples it is possible to simulate an incoherent response of the system. For this reason, the unit cell of the device, as seen in figure 3 was divided into 12 areas, each with a dipole position in the centre. This means that $12 \times 3 = 36$ simulations were run and summed to calculate the resulting response.

The symmetric placement of dipoles in figure 3 might have resulted in an unrealistic result as this symmetry is highly unlikely in a real device. To test for the accuracy of the results, random dipole positions

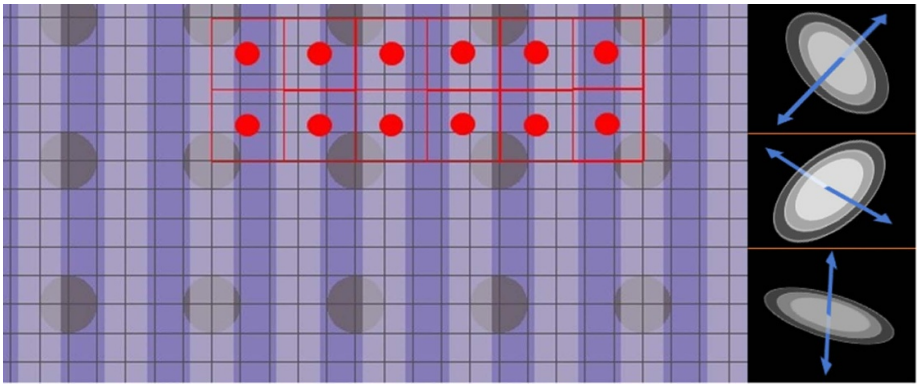

Figure 3. The QLED cross section as seen from the top, divided into dipole areas and the three different dipole orientations.

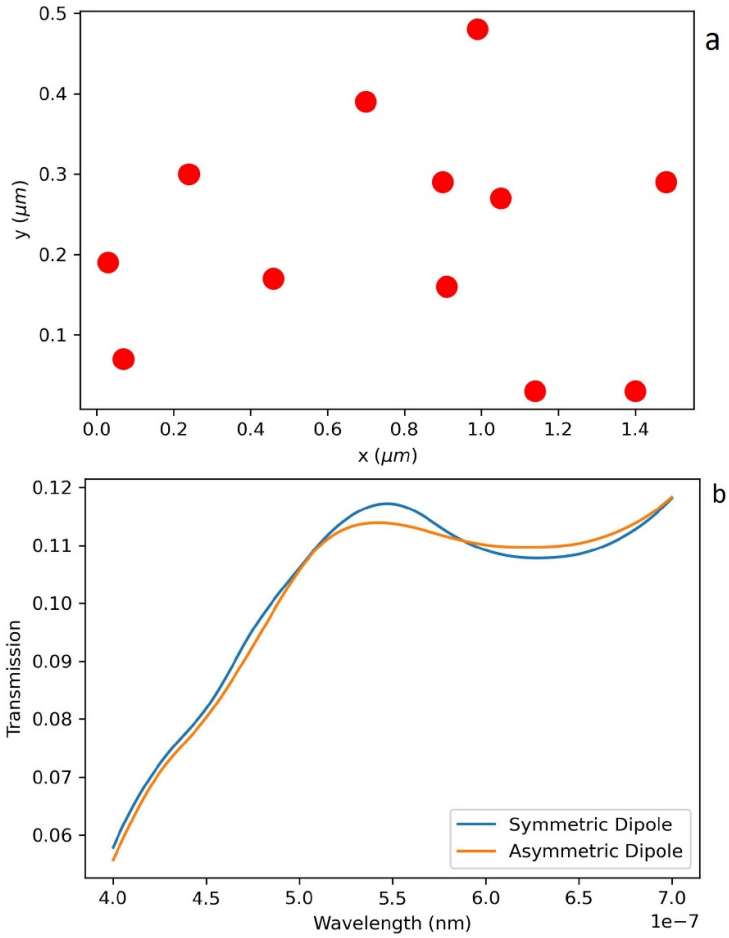

Figure 4. (a) Randomly selected dipole positions for simulating the unit cell and (b) the transmission comparison of the symmetrically and randomly placed dipole simulations.

were chosen for the unit cell and the simulation was run again to test for the effect of asymmetric dipole positions. The dipole positions can be seen in figure 4(a) where the *x* and *y*-axes are the height and width of the unit cell shown in figure 3. The results can be seen in figure 4(b). Although the transmission spectra did not change significantly with the use of asymmetric dipoles, the slight changes may suggest that the symmetrical dipole placement may have an effect in the LEE and this will be explored further in our future works.

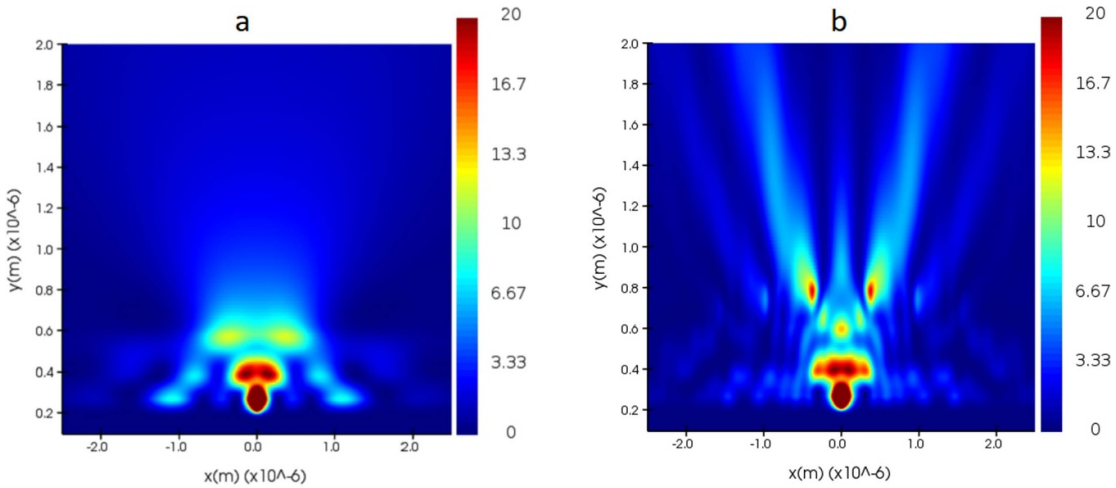

Figure 5. The E^2 field intensity profile of the reference device (a) and the device with the nanopillar array and gratings (b). The y-axis is the direction of the stack (z-direction) and x-axis is the x-direction. The colour scale is arbitrarily chosen for better comparison.

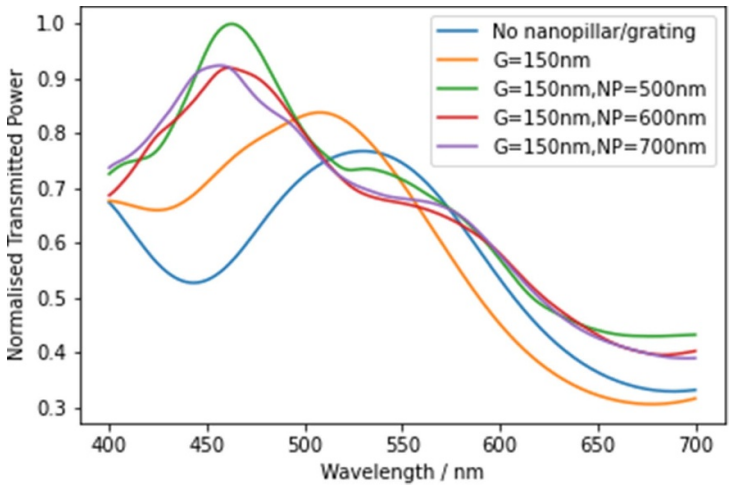

Figure 6. The normalised power extracted from the reference device, the device with a grating structure with a width and separation of 150 nm and nanopillar arrays with different pitch values.

5. Results and discussion

To start with, a 2D FDTD simulation was run with the same structure stacked in the y-axis and a 2D frequency domain profile and power monitor was placed in the x–y plane to measure the E^2 field intensity inside and outside the reference device compared to the nanopillar and grated device. A single dipole was placed inside the EML and the resulting field profile is shown in figure 5. It can be seen that without the nanopillars, most of the light is stuck in the device stack in various layers in figure 5(a). The nanopillar and the grating structure help extract this light into air, which can be seen in figure 5(b). Both profiles are colour scaled to the same arbitrary number for better comparison.

Another experiment that was done with the 2D FDTD was to see the effects of adding the grating structure and the nanopillar arrays. The results are shown in figure 6. Compared to the reference device, adding gratings to the ITO/glass interface increases the LEE in the blue region (400 nm to ∼540 nm), after which decreases the efficiency. Adding nanopillar arrays further increases the LEE in the blue region (400–540 nm) as well as makes the device more efficient in the red region (600–700 nm) when compared to the reference device. The combination which gave the best results was a grating structure with a width and separation of 150 nm and a nanopillar array with a pitch of 500 nm. For these experiments, the nanopillar widths and heights were kept at 200 nm.

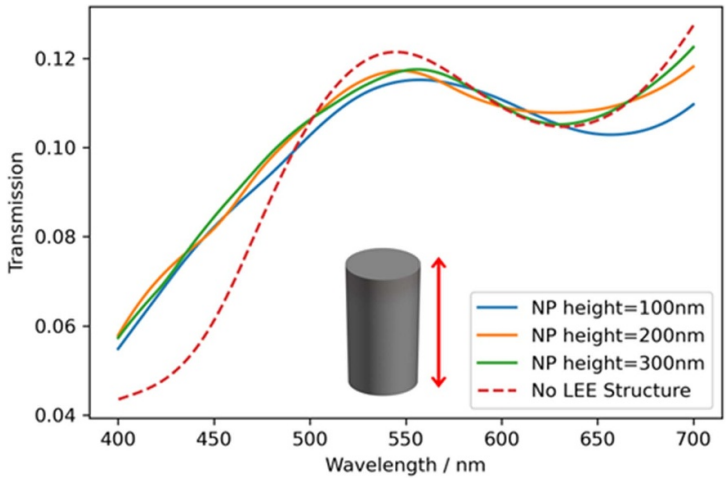

Figure 7. The transmission through the QLED stack at different wavelengths for different heights with a nanopillar pitch of 500 nm and a nanopillar radius of 100 nm.

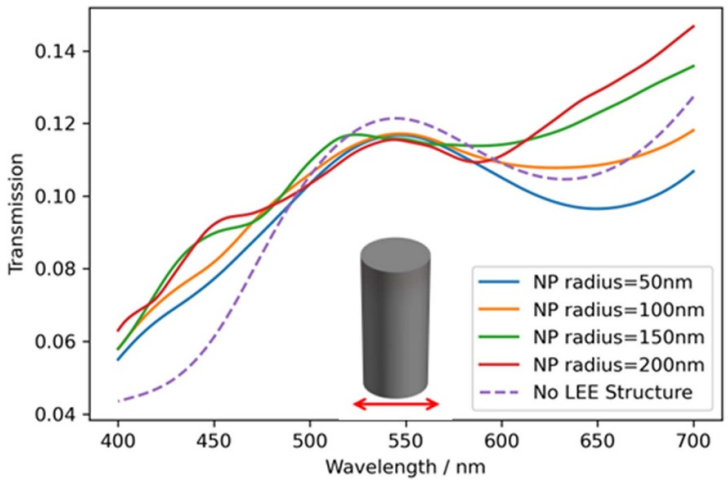

Figure 8. The transmission through the QLED stack at different wavelengths for different nanopillar widths with a pitch of 500 nm and a height of 200 nm.

Afterwards, the 3D FDTD simulations were run as described in section 3 to obtain more accurate and reliable results regarding the device performance. A 2D frequency domain profile and power monitor was placed in the *x*–*y* plane about one micrometer above and perpendicular to the device stack. This allowed monitoring of all the electromagnetic power reaching out above the device, making it out into the air. The first variable tested was changing the heights of the nanopillar arrays while keeping the 500 nm pitch and 100 nm radius. The results are shown in figure 7. It is important to note that the *y*-axis here is the transmission and not the power. The main enhancement occurs in the blue region (400–500 nm). At 400 nm, the enhancement for 100 nm, 200 nm and 300 nm is 26%, 33% and 32% respectively when compared to the reference device. There is more change in the transmission in the red region as the height changes. However, the transmission is still lower when compared to the reference device.

Continuing with the same setup, the nanopillar pitch was kept at 500 nm, heights were set to 200 nm and the nanopillars' radius varied. The results are shown in figure 8. For smaller nanopillar widths the enhancement is only observed in the blue region. However, increasing the nanopillar width up to 400 nm increases the enhancement in the blue region as well as increasing the enhancement in the red region. For a nanopillar width of 400 nm, the enhancement at 400 nm is as high as 45% and this number is 27% for a nanopillar width of 100 nm. The light extracted at 700 nm also increases by 15% for the 400 nm width nanopillars. The enhancement reaches up to 50% around 460 nm and up to 20% around 640 nm, which are the wavelengths used for commercialised blue and red devices respectively.

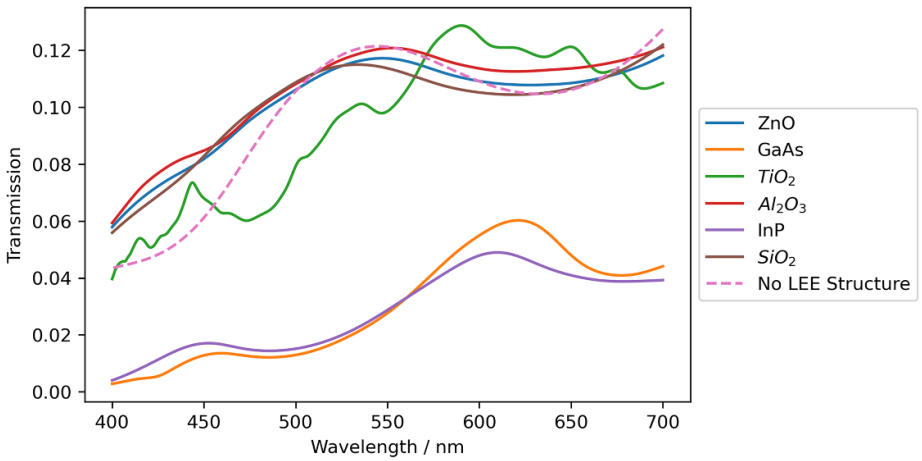

Figure 9. Transmission through a QLED stack at different wavelengths for different nanopillar materials.

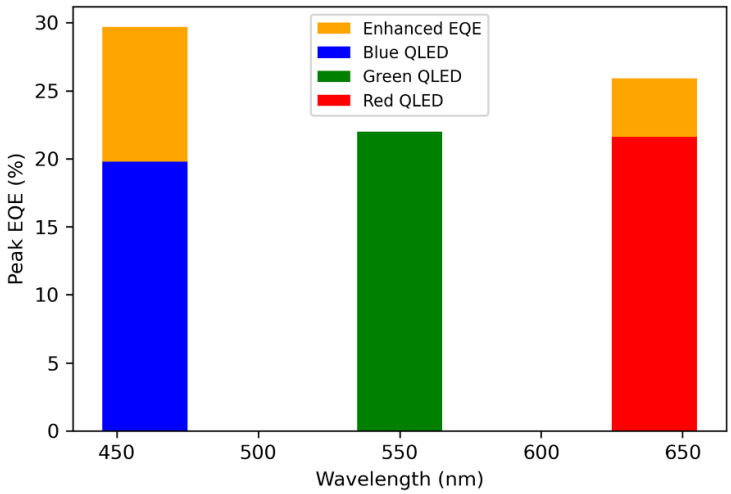

Figure 10. The theoretical increase due to the presence of the photonic structures in peak EQEs stated in the literature.

The final study that was conducted was changing the nanopillar materials to see how this would affect light extraction. A set of materials was chosen in order to have a range of bandgaps and refractive indices. All of the nanopillar dimensions for these materials were set at 500 nm pitch, 200 nm height and 100 nm radius. The results are shown in figure 9. It is clearly observed that the two lower bandgap materials, InP at ∼1.3 eV and GaAs at ∼1.4 eV, decreased the total light extracted significantly. The two reasons behind this are the bandgap falling into the IR region and absorbing most of the visible light and the high refractive indices creating too much contrast between the glass/nanopillar and nanopillar/air interface. The other 4 larger bandgap materials, TiO_2 at ∼3.2 eV, ZnO at ∼3.4 eV, Al_2O_3 at ∼7.0 eV and SiO_2 at ∼8.9 eV all increased the LEE at particular regions. At 400 nm, ZnO, Al_2O_3 and SiO_2 increased the amount of light extracted by 33%, 36% and 29% respectively. TiO_2 on the other hand, increased the LEE in the ∼590 nm region significantly, which was not observed by any of the other materials. This can be due to the refractive index of TiO_2. Since their refractive index does not change significantly over the visible light region, the high bandgap materials' refractive indices were modelled as constant by Lumerical. However, this was not the case with TiO_2 and its refractive index was modelled as a variable, which we believe is the cause for the peaks and dips in its transmission spectra.

The peak EQEs for blue, green and red emitting QLEDs in literature are 19.8%, 22.9% and 21.6% respectively [57–59]. These EQEs are achieved by optimizing the device structure and charge balance. With the improvement in the LEE, the theoretical EQEs of these devices can further be increased. Figure 10 shows these devices' theoretical EQEs with the photonics structures. The max EQE can be enhanced up to 29.7%

and 25.9% in blue and red devices respectively. The LEE increase in the green region (∼540 nm) was not observed in this study and remains a challenge using these photonic structures.

6. Conclusions

The 2D FDTD results showed that adding a grating structure to the ITO/glass interface and a nanopillar structure on top of the device increased the LEE in the blue region significantly. This was also visually observed by the E^2 intensity profiles showing more light making its way into air with the nanopillar array and grating structured device. 3D simulations were also run to make the results more reliable. It was observed that the grating and the nanopillar structure improve the light extraction, especially in the 400–500 nm region. This is of particular importance due to the blue QLED devices suffering from lower efficiency compared to their red and green counterparts [59]. In addition, a high voltage is normally required to achieve targeting lumens, which significantly reduces the lifetime.

3D simulations showed that changing the nanopillar material and dimensions can help extract light from different spectral regions. It was shown that changing the heights of the nanopillars made very little difference in the LEE. More significant changes were observed by increasing the nanopillar widths. Using ZnO nanopillars of 500 nm pitch, 200 nm height and 400 nm width can increase the LEE efficiency at 400 nm and 460 nm by 45% and 50% respectively and at 640 nm and 700 nm by 20% and 15% respectively. It was also shown that using low-bandgap materials for nanopillars decreased the LEE due to high refractive index contrast and absorption in the visible spectrum. On the other hand, high bandgap materials increased the LEE compared to the reference device. In particular, TiO_2 nanopillars increased the transmission in the ∼590 nm region, which was not observed significantly for other materials. We believe that it should be possible to increase the LEE in different spectral regions by choosing the correct combination of the nanopillar dimensions and the materials used.

Data availability statement

The data that support the findings of this study are available upon reasonable request from the authors.

Acknowledgments

We would like to thank EPSRC SWIMS (EP/V039717/1), EPSRC CDT in Compound Semiconductor Manufacturing (EP/S024441/1) and Huawei Cambridge for funding this project.

ORCID iDs

Julia A Weinstein https://orcid.org/0000-0001-6883-072X
Bo Hou https://orcid.org/0000-0001-9918-8223

References

[1] Li B *et al* 2020 Colloidal quantum dot hybrids: an emerging class of materials for ambient lighting *J. Mater. Chem.* C **8** 10676–95
[2] Osypiw A R C *et al* 2022 Solution-processed colloidal quantum dots for light emission *Mater. Adv.* **3** 6773–90
[3] Bardsley J N 2004 International OLED technology roadmap *IEEE J. Sel. Top. Quantum Electron.* **10** 3–9
[4] Monkman A 2022 Why do we still need a stable long lifetime deep blue OLED emitter *ACS Appl. Mater. Interfaces* **14** 20463–7
[5] Sudheendran Swayamprabha S *et al* 2021 Approaches for long lifetime organic light emitting diodes *Adv. Sci.* **8** 2002254
[6] Laaperi A 2008 OLED lifetime issues from a mobile-phone-industry point of view *J. Soc. Inf. Disp.* **16** 1125–30
[7] Baskoutas S and Terzis A F 2006 Size-dependent band gap of colloidal quantum dots *J. Appl. Phys.* **99** 013708
[8] Ramasamy P, Kim N, Kang Y S, Ramirez O and Lee J S 2017 Tunable, bright and narrow-band luminescence from colloidal indium phosphide quantum dots *Chem. Mater.* **29** 6893–9
[9] Jun S and Jang E and 2013 Bright and stable alloy core/multishell quantum dots *Angew. Chem., Int. Ed.* **125** 707–10
[10] Rizzo A *et al* 2008 Hybrid light-emitting diodes from microcontact-printing double-transfer of colloidal semiconductor CdSe/ZnS quantum dots onto organic layers *Adv. Mater.* **20** 1886–91
[11] Kang Y *et al* 2017 Quantum dots for wide color gamut displays from photoluminescence to electroluminescence *Nanoscale Res. Lett.* **12** 154
[12] Azar K 2000 Power consumption and generation in the electronics industry. A perspective *16th Annual IEEE Semiconductor Thermal Measurement and Management Symp. (Cat. No.00CH37068)* pp 201–12
[13] European Commission Joint Research Centre 2021 Update on the status of LED-lighting world market since 2018 *Technical Report* (Publications Office)
[14] Cheng C *et al* 2022 Balancing charge injection in quantum dot light-emitting diodes to achieve high efficiency of over 21 *Sci. China Mater.* **65** 1882–9

[15] Yu H *et al* 2022 High-efficiency, large-area, flexible top-emitting quantum-dot light-emitting diode *ACS Photonics* (https://doi.org/10.1021/acsphotonics.2c00863)
[16] Tan G *et al* 2016 High ambient contrast ratio OLED and QLED without a circular polarizer *J. Phys. D: Appl. Phys.* **49** 315101
[17] Watanabe S *et al* 2003 Internal quantum efficiency of highly-efficient In_x Ga_{1-x} N-based near-ultraviolet light-emitting diodes *Appl. Phys. Lett.* **83** 4906–8
[18] Liu Z, Li F, Huang G, Wei J, Jiang G and Huang Y 2020 Enhance the light extraction efficiency of qled with surface micro-nanostructure *J. Nanomaterials* **2020** e8858996
[19] Choi J *et al* 2018 Light extraction enhancement in flexible organic light-emitting diodes by a light-scattering layer of dewetted Ag nanoparticles at low temperatures *ACS Appl. Mater. Interfaces* **10** 32373–9
[20] Wang Y *et al* 2020 Efficient structure for InP/ZnS-Based electroluminescence device by embedding the emitters in the electron-dominating interface *J. Phy. Chem. Lett.* **11** 1835–9
[21] Mashford B S *et al* 2013 High-efficiency quantum-dot light-emitting devices with enhanced charge injection *Nat. Photon.* **7** 407–12
[22] Tu N, Kwok Z H E and Lee S W R 2018 Quantum dot light emitting diodes based on ZnO nanoparticles *2018 20th Int. Conf. on Electronic Materials and Packaging (EMAP)* pp 1–4
[23] Caruge J M, Halpert J E, Wood V, Bulović V and Bawendi M G 2008 Colloidal quantum-dot light-emitting diodes with metal-oxide charge transport layers *Nat. Photon.* **2** 247–50
[24] Chen Z and Chen S and 2022 Efficient and stable quantum-dot light-emitting diodes enabled by tin oxide multifunctional electron transport layer *Adv. Opt. Mater.* **10** 2102404
[25] Kim M *et al* 2021 High-efficiency quantum dot light-emitting diodes based on Li-doped TiO_2 nanoparticles as an alternative electron transport layer *Nanoscale* **13** 2838–42
[26] Kim H M, ARbM Y, Kim T W, Seol Y G, Kim H P and Jang J 2014 Semi-transparent quantum-dot light emitting diodes with an inverted structure *J. Mater. Chem C* **2** 2259–65
[27] Li Z 2017 Enhanced performance of quantum dots light-emitting diodes: the case of Al_2O_3 electron blocking layer *Vacuum* **137** 38–41
[28] Palik E D 1998 *Handbook of Optical Constants of Solids* (New York: Academic)
[29] Kirkwood N, Singh B and Mulvaney P 2016 Enhancing quantum dot LED efficiency by tuning electron mobility in the ZnO electron transport layer *Adv. Mater. Interfaces* **3** 1600868
[30] Guo S *et al* 2021 boosting efficiency of InP quantum dots-based light-emitting diodes by an in-doped ZnO electron transport layer *IEEE Electron Device Lett.* **42** 1806–9
[31] Stelling C, Singh C R, Karg M, TAF K, Thelakkat M and Retsch M 2017 Plasmonic nanomeshes: their ambivalent role as transparent electrodes in organic solar cells *Sci. Rep.* **7** 42530
[32] Fang T, Wang T, Li X, Dong Y, Bai S and Song J 2021 Perovskite QLED with an external quantum efficiency of over 21% by modulating electronic transport *Sci. Bull.* **66** 36–43
[33] Cho H *et al* 2020 Highly efficient deep blue cd-free quantum dot light-emitting diodes by a p-type doped emissive layer *Small* **16** 2002109
[34] Pidluzhna A *et al* 2019 Multi-channel electroluminescence of CdTe/CdS core-shell quantum dots implemented into a QLED device *Dyes Pigments* **162** 647–53
[35] Ninomiya S and Adachi S 1995 Optical properties of cubic and hexagonal CdSe *J. Appl. Phys.* **78** 4681–9
[36] Santaella J J, Critchley K, Rodríguez-Bolívar S and Gómez-Campos F M 2020 Design and fabrication of $CuInS_2$/ZnS-based QLED for automotive lighting systems *Nanotechnology* **32** 105204
[37] Kim S K, Kim J H, Yang H S and Kim Y S 2018 P-112: a Study on the effect of electrical characteristics of HTL on electrical properties of qled and its efficiency *SID Symp. Digest of Technical Papers* vol 49 pp 1632–5
[38] Yang X *et al* 2014 Light extraction efficiency enhancement of colloidal quantum dot light-emitting diodes using large-scale nanopillar arrays *Adv. Funct. Mater.* **24** 5977–84
[39] Vos M F J, Macco B, Thissen N F W, Bol A A and Kessels W M M E 2016 Atomic layer deposition of molybdenum oxide from $(N^tBu)_2$ $(NMe_2)_2Mo$ and O_2 plasma *J. Vac. Sci. Technol. A* **34** 01A103
[40] Lai K Y *et al* 2022 Patterned-bank-free electroluminescent quantum dot emitting array for passive-matrix qled display *Adv. Mater. Technol.* **7** 2100889
[41] Yao L *et al* 2017 fully transparent quantum dot light-emitting diode with a laminated top graphene anode *ACS Appl. Mater. Interfaces* **9** 24005–10
[42] Chen Q *et al* 2020 Gate-tunable all-inorganic QLED with enhanced charge injection balance *J. Mater. Chem.* C **8** 1280–5
[43] TAF K *et al* 2014 Electrically tunable plasmonic behavior of nanocube-polymer nanomaterials induced by a redox-active electrochromic polymer *ACS Nano* **8** 6182–92
[44] Salehi A, Fu X, Shin D H and So F 2019 Recent advances in OLED optical design *Adv. Funct. Mater.* **29** 1808803
[45] Ho H P and Lam W W 2003 Application of differential phase measurement technique to surface plasmon resonance sensors *Sens. Actuators* B **96** 554–9
[46] Zeng S, Baillargeat D, Ho H P and Yong K T 2014 Nanomaterials enhanced surface plasmon resonance for biological and chemical sensing applications *Chem. Soc. Rev.* **43** 3426–52
[47] Barnes W L 2004 Turning the tables on surface plasmons *Nat. Mater.* **3** 588–9
[48] Brütting W, Frischeisen J, Schmidt T D, Scholz B J and Mayr C 2013 Device efficiency of organic light-emitting diodes: progress by improved light outcoupling *Phys. Status Solidi* a **210** 44–65
[49] Qu Y, Kim J, Coburn C and Forrest S R 2018 efficient, nonintrusive outcoupling in organic light emitting devices using embedded microlens arrays *ACS Photonics* **5** 2453–8
[50] Chang H W *et al* 2013 Nano-particle based scattering layers for optical efficiency enhancement of organic light-emitting diodes and organic solar cells *J. Appl. Phys.* **113** 204502
[51] Qiao D, Li K, Copner N, Gong Y and Chen G 2019 The enhanced light extraction top-emitting organic light-emitting diode based on metallic grating anode *2019 IEEE Int. Conf. on Manipulation, Manufacturing and Measurement on the Nanoscale (3M-NANO)* pp 49–52
[52] Lim T B, Cho K H, Kim Y H and Jeong Y C 2016 Enhanced light extraction efficiency of OLEDs with quasiperiodic diffraction grating layer *Opt. Express* **24** 17950–9
[53] Yee K 1966 Numerical solution of initial boundary value problems involving maxwell's equations in isotropic media *IEEE Trans. Antennas Propag.* **14** 302–7

[54] Cho Y, Pak S, Li B, Hou B and Cha S 2021 Enhanced direct white light emission efficiency in quantum dot light-emitting diodes via embedded ferroelectric islands structure *Adv. Funct. Mater.* **31** 2104239
[55] Cho Y *et al* 2021 Balanced charge carrier transport mediated by quantum dot film post-organization for light-emitting diode applications *ACS Appl. Mater. Interfaces* **13** 26170–9
[56] Cho S B, Sohn J I, Lee S S, Moon S G, Hou B and Park I K 2021 Colour-encoded electroluminescent white light-emitting diodes enabled using perovskite–Cu–In–S quantum composites *J. Mater. Chem.* C **9** 7027–34
[57] Dai X *et al* 2014 Solution-processed, high-performance light-emitting diodes based on quantum dots *Nature* **515** 96–99
[58] Shen H *et al* 2019 Visible quantum dot light-emitting diodes with simultaneous high brightness and efficiency *Nat. Photon.* **13** 192–7
[59] Wang L *et al* 2017 Blue quantum dot light-emitting diodes with high electroluminescent efficiency *ACS Appl. Mater. Interfaces* **9** 38755–60